Solar Adaptive Optics System by Use of Electromagnetic Deformable Mirror

Noriaki Miura [*], Yuuki Noto, Shuusuke Kato, Fumihito Yokoyama, Susumu Kuwamura, Naoshi Baba [1], Yoichiro Hanaoka [2], Shin'ichi Nagata [3], Satoru Ueno [3], Reizaburou Kitai [3], Kiyoshi Ichimoto [3] and Hideki Takami [4]

Department of Computer Sciences, Kitami Institute of Technology, 165 Koen-cho, Kitami, Hokkaido 090-8507, Japan

[1] Department of Applied Physics, Graduate School of Engineering, Hokkaido University, Sapporo, 060-8628, Japan

[2] National Astronomical Observatory of Japan, 2-21-1 Osawa, Mitaka, Tokyo 181-8588, Japan

[3] Hida Observatory, Graduate School of Science, Kyoto University, Kamitakara, Takayama, Gifu 506-1314, Japan

[4] Subaru Telescope, National Astronomical Observatory of Japan, 650 North A'ohoku Place, Hilo, HI 96720, USA

Abstract

A solar adaptive optics system has been improved by both using a high-speed electromagnetic deformable mirror and adopting a modified sum-of-absolute-differences algorithm in wavefront sensing. Results of laboratory experiments clearly show that the use of the mirror raises the temporal performance of the system. In solar observations, wavefront compensation using solar granules as a target is realized.

KEYWORDS: adaptive optics, solar observation

[*] E-mail address: miura@cs.kitami-it.ac.jp

1. Introduction

Several solar observatories equip adaptive optics (AO) systems for high-resolution imaging from the ground [1-4]. We are developing a solar AO system for the domeless solar telescope at the Hida Observatory in Japan [5-7]. Our first system was designed to compensate low-order wavefront phases in rather short wavelength of about 430 nm, using a deformable mirror (DM) with nineteen piezo-actuators and a Shack-Hartmann wavefront sensor with a 5x5 microlens array [5, 6]. Although the system worked as expected, its capability of spatially correcting wavefront was insufficient. In our second system, we used a DM with 52 electromagnetic actuators, and succeeded in raising the quality of images obtained with AO system in case of slow turbulence [7]. Temporal performance of the electromagnetic DM was, however, such that it could not correct rapidly-varying wavefront.

To improve the system further, we have introduced two major modifications in the present system: the replacement of the DM and the use of a sum-of-absolute-differences (SAD) algorithm [8] for measuring image shifts in wavefront sensing. Recently, a high-speed model of the electromagnetic DM becomes commercially available, whose bandwidth in dynamic response is improved from 250 Hz to 1 kHz [9]. This mirror has not been used for astronomical purposes, yet, to our knowledge.

Since our second system, we have adopted the technique of Zernike-modal control for driving the DM, in which voltages applied to actuators are the linear sums of Zernike-modal patterns. This technique allows stable control of the mirror even when

severe turbulence locally exists, and is also useful to control the high-speed DM. We briefly review the technique of Zernike-modal control.

In Shack-Hartman wavefront sensors, wavefront slopes are measured through detecting displacements of a target pattern on subapertures. In our previous systems, a sunspot was used as a target because its contrast is so high that the detection of its centroid is possible. However, there was a serious problem that sunspots neither always appear nor exist everywhere on the solar surface.

This problem can be solved if granulation is used as a target, because solar granules always exist over the solar surface. The contrast of granulation is, however, so low that centroiding is unavailable for wavefront sensing. As alternative methods, there are a standard crosscorrelation technique [4] and the SAD algorithm [8]. We decided to use the latter because of less computational complexity. We describe a modified technique of the SAD algorithm.

In this paper, we investigate the performance of our new system through laboratory experiments and apply it to solar observations at the Hida observatory.

2. AO system

Our AO system is composed of two closed-loop units of correcting image shifts and image degradation, which are individually controlled by two standard PCs. The frame rates of sensing cameras are both 955. Its design policy is categorized in the so-called low-cost type [8,10] and unchanged since our first system. System configuration is almost same as described in the reference [7]: we just replaced the DM to a high speed one. The dynamic response of the high-speed DM rises by a factor of four, while other

parameters are not changed: it has a continuous surface supported by a circular edge and deformed by 52 voice-coil actuators. The separation between actuators is 2.5 mm and the aperture size is 15mm. In our system, the diameter of the pupil image on this mirror is designed to be 13.0 mm. Positional relations of the DM actuators with Zernike polynomials are shown in Fig, 3 of the reference [7]. They show that higher-order terms have fine and steep changes between actuators.

3. Modal control of deformable mirror

The way how to expand wavefront phases with Zernike coefficients is known well [11]. A vector $\boldsymbol{a}$ of Zernike coefficients is related to a measurement vector $\boldsymbol{g}$ of image shifts by

$$\boldsymbol{g} = \boldsymbol{\Gamma a} \quad , \tag{1}$$

where $\boldsymbol{\Gamma}$ is the matrix whose elements are partial derivations of Zernike polynomials.

In modal control of a mirror in our system, the shape of mirror surface is assumed to be the linear sum of Zernike-modal patterns. Also, the mirror response is supposed to be linear to the voltage applied. Therefore, voltage vector $\boldsymbol{v}$ is represented by

$$\boldsymbol{v} = \boldsymbol{ZCa} \ , \tag{2}$$

where $\boldsymbol{Z}$ is the matrix whose elements are Zernike coefficients. The matrix $\boldsymbol{C}$ is diagonal and its elements specify the response of the mirror surface to voltages applied in each Zernike mode.

The j-th element c_j in $\boldsymbol{C}$ is experimentally determined as follows: we set the j-th element a_j in $\boldsymbol{a}$ to unity and the others to zero, and then calculate an ideal measurement vector $\boldsymbol{g}$ using Eq. (1). Next, using the same $\boldsymbol{a}$ and assuming $\boldsymbol{C}$ to be the unit matrix, we

obtain voltages to be applied using Eq. (2). These voltages are actually applied to the DM and then image shifts are measured with the wavefront sensor to give an actual measurement vector $\boldsymbol{g}'$. We define the error between the ideal and actual measurement vectors by

$$E_j = \left\| \boldsymbol{g} - c_j \boldsymbol{g}' \right\| / \left\| \boldsymbol{g} \right\| \quad , \tag{3}$$

where || . || denotes norm. Using the least square procedure, we minimize E_j to obtain c_j.

Figure 1 shows errors E_j in the first twenty Zernike modes except for piston. As can been seen, they are notably large in Zernike modes higher than nine. This is because higher-order terms have fine and steep variations in their shapes which are hardly formed by the DM. As a consequence, we decided to use lower nine Zerinike modes.

4. Modified SAD technique for wavefront sensing

Figure 2(a) is an image acquired with the wavefront sensor. The size of a subaperture is 42x42 pixels^2, corresponding to 28.7x28.7 arcsec^2. The task of the sensor is to detect relative shifts between sub-images on subapertures. The central part $r(x,y)$ of a sub-image is used as a target for measuring image shifts on the other subapertures. A sub-image $s(x,y)$ on every subaperture is scanned with the target image, being evaluated with the sum of absolute values of differences between their images:

$$p(u,v) = \sum_R \left| s(x-u, y-v) - r(x,y) \right| \quad , \tag{4}$$

where R denotes the region of $r(x,y)$. The position of the minimum in $p(u,v)$ gives a shift vector as a result. In our observations, we set the sizes of a target image and a scan area to 13x13 and 11x11 pixels^2, respectively.

Ordinarily, interpolation is needed to determine the amount of a sub-pixel shift because the scan can be done pixel by pixel. However, a standard linear interpolation procedure frequently did not work well in our observations. We think that this is because it was sensitive to the change of a target shape induced by local seeing variation.

We hence used another technique as follows: the two-dimensional distribution of SAD $p(u,v)$ was inverted and subtracted by $\alpha\times$(maximum value), and then resultant negative values were forced to be zero. The coefficient α ($0< \alpha <1$) should be set to larger so that pixel values remain as non-zero only around the maximum. We used α=0.85 in our observations. Such processes usually yield, as a result, a spot on a subaperture, as shown in Fig. 2(b). The centroids of all the spots are then detected to determine the measurement vector. Variation of spot shapes in Fig. 2(b) arose from deformation of target patterns according to local variation of seeing. Despite of such target-deformations, our modified technique enables the measurement of target shifts in a sub-pixel unit.

5. Laboratory experiments

We put our AO system behind a simulated atmosphere-telescope system and then conducted experiments. The simulated atmosphere-telescope system used comprises a deformable mirror, referred to as a perturbation mirror, for causing wavefront errors onto a plane wave from a He-Ne laser, a pinhole as an object, and a lens as a primary mirror of the telescope. The perturbation mirror has a membrane surface and nineteen actuators whose maximum strokes are about 1.5 um. In our experiments, rotating

astigmatism plus defocus was induced into the wavefront phases.

We drove the perturbation mirror with various frequencies to investigate the temporal behavior of the AO system. We acquired 200 images of the laser spot for each frequency, measured the normalized correlation values of every two neighboring images, and then calculated their average. If the AO system perfectly worked, crosscorrelation values between frames should always be unity. Columns 3 and 4 in Table 1 list the average crosscorrelation values obtained without and with AO, respectively. Over all the frequencies, the use of AO greatly improved the correlation values. The table also shows the comparison between the original and the high-speed DMs. The use of the high-speed DM significantly raised the correlation values especially in higher frequencies.

All the correlation values obtained without AO using the high-speed DM are larger than those using the original DM, as shown in Table 1. These results were due to the individual differences in the initial precision of mirror flatness. More fixed aberration attends the high-speed DM used, and hence the influence of additional wavefront errors into image variation was relatively smaller. The correlation values became higher as a consequence.

To examine the imaging performance, we added 200 frames to make a long-exposure image, and then calculated its Strehl ratio. The Strehl ratios listed in columns 4 and 5 in Table 1 are normalized with those of perturbation-free laser spots. Improvement of image quality by AO is obvious. Similarly to the correlation values, the Strehl ratios rose by use of the high speed DM. In addition, the Strehl ratios obtained without AO show the same tendency as the correlation values. Since the Strehl ratio of a perturbation-free laser spot through the original DM was larger according to the

precision of mirror surface, Strehl ratios normalized with it became smaller.

5. Solar observations

We conducted solar observations at the Hida Observatory in September 1, 2008. The observational wavelength was 430.6 nm (bandpass of 2 nm). We turned AO on/off during the acquisition of 300 images with the frame rate of 28 Hz. We compared image variations with and without AO by evaluating crosscorrelations between frames. An ideal AO could yield temporarily constant correlation values of unity. As expected, the use of AO suppressed image variation as shown in Fig. 3. However, the effect of AO was sometimes violated, for example, within frames 50-70 in Fig. 3(a). Such violation was caused by instantly severe seeing variation.

To compare the quality of images, we made long-exposure images by adding 50 frames. In Fig. 4, the long exposure images with AO shown in the right row reveal finer structures than those without AO. In particular, we can observe the temporal change of granulation itself between 1:04 and 1:06.

6. Conclusions

In the present AO system, two major modifications were introduced: the replacement of the DM and the use of a modified SAD algorithm in measuring image shifts with a wavefront sensor. The former greatly improved the temporal performance of the system and the latter allows wavefront compensation using solar granulation as a target for wavefront sensing. These are significant advances toward a useful AO system for

high-resolution solar imaging.

Acknowledgments

N. Miura specially thanks to F. Rooms of ALPAO for his cooperation. This work was partially supported by both a Grant-in-Aid for Scientific Research (B) from the Japan Society for the Promotion of Science (No.19340042) and a foundation for Joint-Research Development from the National Astronomical Observatory of Japan.

References

1. T. R. Rimmele: Proc. SPIE **5490** (2004) 34.
2. G. Moretto, M. Langlois, K. Richards, S. Hegwer, D. Gilliam, and T. Rimmele: Proc. SPIE **5490** (2004) 905.
3. G. B. Scharmer, P. Dettori, M. G. Löfdahl, and M. Shand: Proc. SPIE **4853** (2003) 370.
4. T. Berkefeld, D. Soltau, and O. von der Lühe: Proc. SPIE **5903** (2005) 59030O.
5. N. Miura, T. Kobayashi, S. Sakuma, S. Kuwamura, N. Baba, Y. Hanaoka, S. Ueno, and R. Kitai: Opt. Rev. **13** (2006) 338.
6. N. Miura, Y. Noto, S. Kato, S. Kuwamura, N. Baba, Y. Hanaoka, S. Ueno, and R. Kitai: Opt. Rev. **14** (2007) 159.
7. N. Miura, Y. Noto, S. Kato, S. Kuwamura, N. Baba, Y. Hanaoka, S. Nagata, S. Ueno, R. Kitai, and H. Takami: Proc. SPIE **7015** (2008) 70156U.
8. C. U. Keller, C. Plymate, and S. M. Ammons: Proc. SPIE **4853** (2003) 351.
9. http://www.alpao.fr/
10. C. Paterson, I. Munro, and J. C. Dainty: Opt. Express **6** (2000) 175.
11. G. Rousset: in *Adaptive Optics in Astronomy* ed. F. Roddier (Cambridge University Press, Cambridge, 1999) *Chap. 5*.

Table 1. Results of laboratory experiments

Deformable Mirror	Perturbation frequency (Hz)	Average crosscorrelation values		Strehl ratios	
		Without AO	With AO	Without AO	With AO
Original DM52	66	0.532	0.874	0.159	0.923
	99	0.538	0.817	0.167	0.720
	130	0.537	0.770	0.161	0.592
	172	0.538	0.724	0.162	0.424
High speed DM52	66	0.652	0.904	0.270	0.946
	99	0.669	0.913	0.268	0.903
	130	0.655	0.904	0.268	0.858
	172	0.649	0.880	0.270	0.769

Figure Captions

Figure 1. Errors between ideal and actual measurement vectors.

Figure 2. (a) image acquired with wavefront sensor and (b) image obtained with a modified SAD technique.

Figure 3. Crosscorrelation values between two neighbor frames. Observational times are denoted in figures. The arrows indicate the period while AO is working.

Figure 4. Long-exposure solar images observed without (in the left row) and with (in the right row) AO. The field of view of these images is 19.0x19.0 arcsec^2.

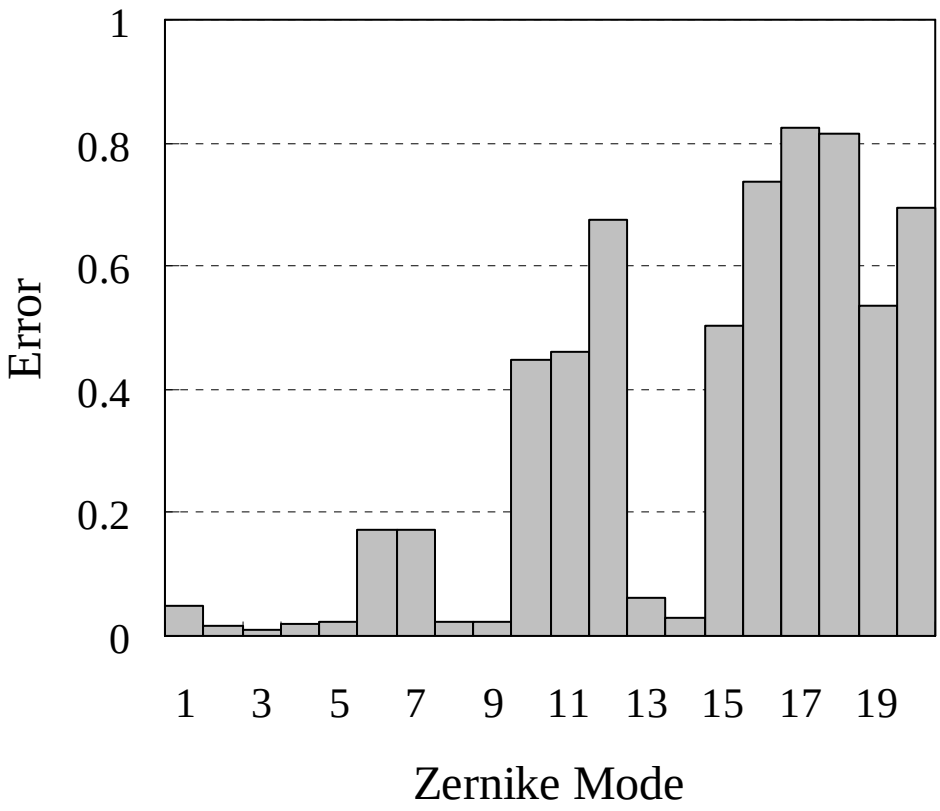

Figure 1. N. Miura

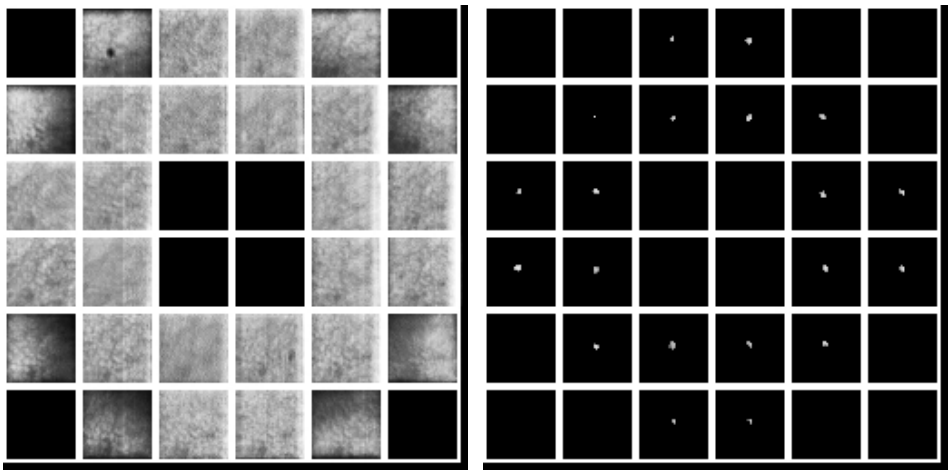

Figure 2. N. Miura

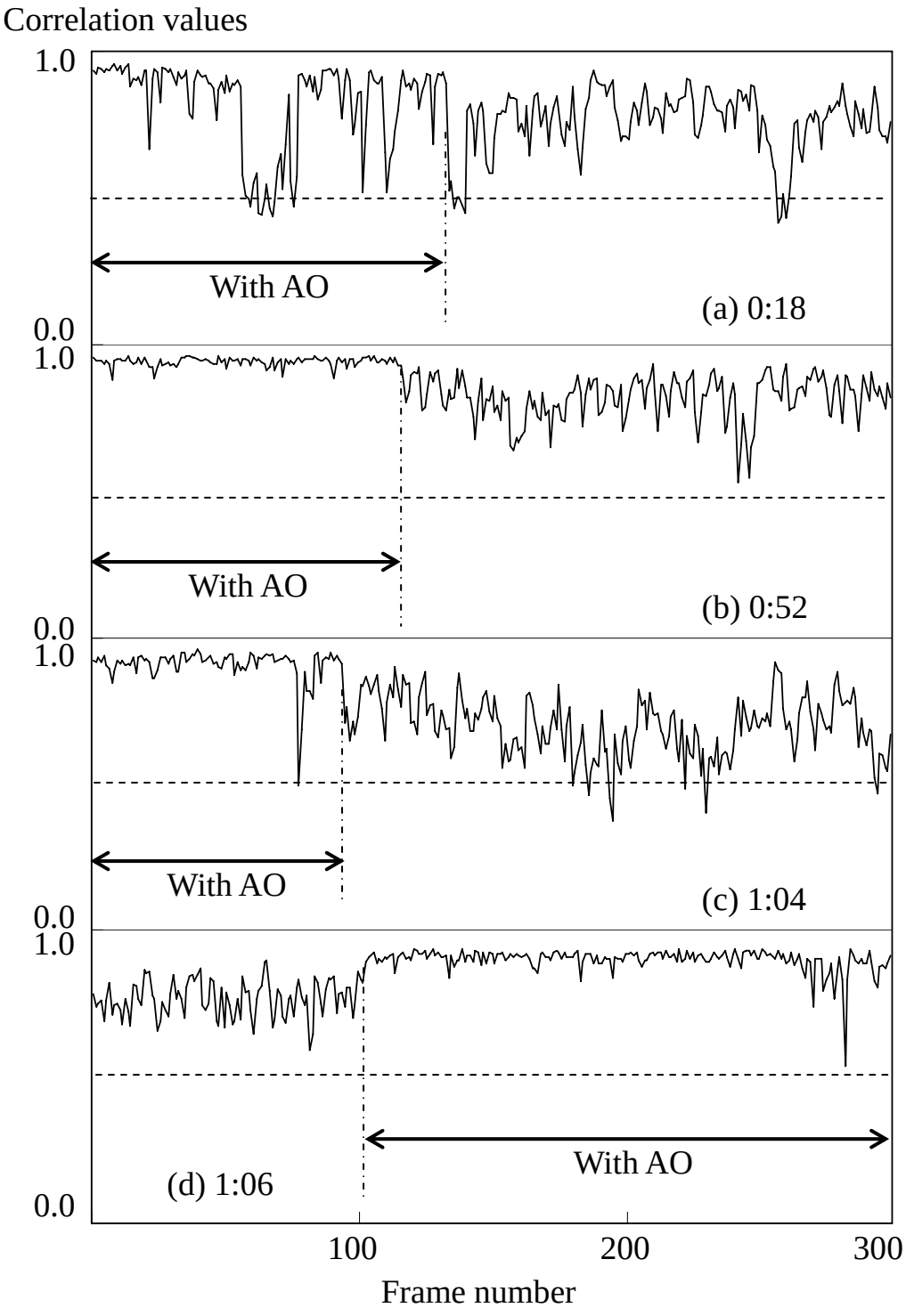

Figure 3. N. Miura

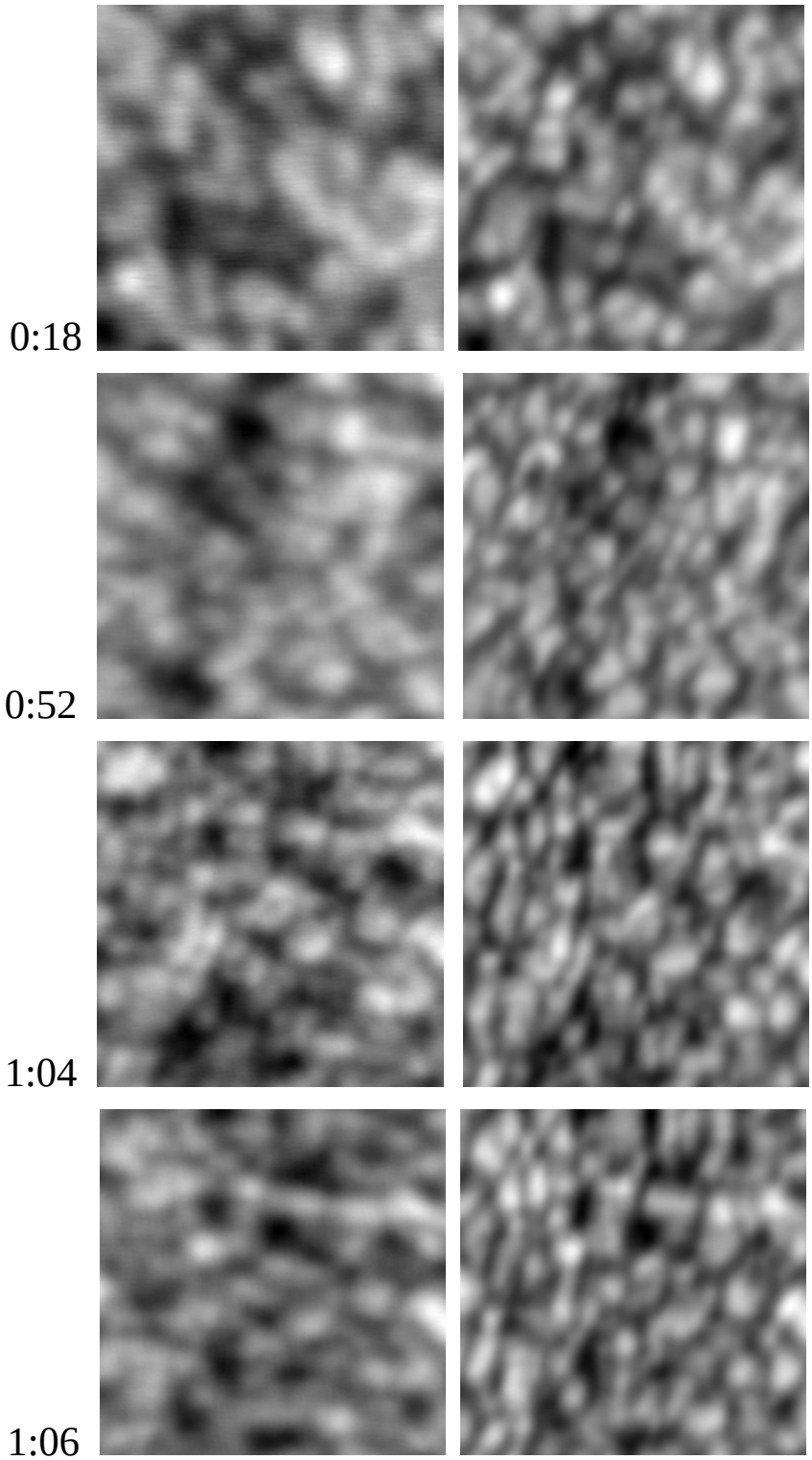

Figure 4. N. Miura